# Numerical investigation of the power performance of a wave energy converter comprising a multi-body power take-off

F. Elefant, A. Babarit, P. Ferrant

*Abstract*—**This article presents a wave energy converter exploiting the pitch of a floating body moored to the seabed. When the floating body tilts under the action of an incoming wave, a movable mass, placed inside the hull, moves relative to the floating body and actuates an electrical generator. Most devices of this type have the drawback that the moving mass sequentially accelerates, slows down, stops and then repeats this sequence in the opposite direction. This generates an irregular instantaneous power output. The proposed concept consists of (at least) two eccentric bodies having the same mass and revolving at opposite speeds around a vertical axis. In this « counter-rotating » solution, the oscillations of the float result in the continuous circular motion of the direct-drive PTO, though the global centre of gravity of the eccentric bodies moves back-and-forth along the symmetry axis of the device. If the eccentric bodies move at constant speed, their global centre of gravity moves in a sinusoidal manner along its pathway. The present study aims to investigate, through modelling and numerical simulations, the influence of the main parameters, such as the phase and the PTO mass moment, on the performance of a counter-rotating device exposed to waves of various heights and various wavelengths. Optimal phase and mass moment are determined numerically. The resulting output power is close to the theoretical maximum power that can be harvested by the floating body.**

***Keywords*— *Numerical simulation, Performance analysis, Renewable energy, Rotating-mass converter, Wave energy converter.***

## I. INTRODUCTION

### A. Background of the study

AMONGST the many devices that have been designed to convert wave energy into electrical energy, various machines make use of the pitch and surge of a moored floating body [1].

One particular type of machines uses the back-and-forth motion of a mass located within the floating body to drive an electrical generator. When the floating body tilts under the action the waves, the mass is drawn by gravity towards the low point of its trajectory. When the floating body tilts in the opposite direction, the mass is drawn back. In some devices of this type, the mass moves back and forth in a straight line [2], [3], while in other devices the mass moves along an arc of a circle [4], [5]. Generally, these devices have the advantage that the Power Take-Off (PTO), is protected by the hull of the floating body. However, these devices have the disadvantage that the drive speed of the PTO varies greatly during each oscillation cycle.

### B. Operating principle of the studied device

One way of solving the aforementioned problem is to replace the longitudinal reciprocating motion of conventional devices by two eccentric bodies rotating at opposite speeds around a vertical axis [6], (see Fig. 1).

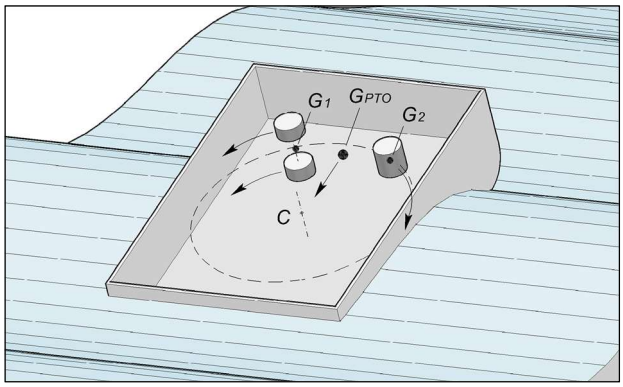


Fig. 1. Implementation principle of a counter-rotating solution.

As illustrated in Fig. 1, the respective centres of gravity ($G_1$ and $G_2$) of the two eccentric bodies move along a horizontal circle with centre $C$. Both bodies have the same mass moment $m_1 r_1 = m_2 r_2$ with respect to the centre $C$ of the circle. Eccentric body 1 is divided in two equal parts,



The present paper completes and extends a research work previously presented in French at the "Journées de l'Hydrodynamique", in Poitiers (France), November 2022. https://jh2022.sciencesconf.org/413358

This work was supported in part by the Association Nationale de la Recherche Technologique (A.N.R.T.) 33 rue Rennequin, F-75017 Paris, France, under grant number 19/0527. This work was financially supported by Énergies de Vagues Et Renouvelables (EVER), 144, rue Paul Bellamy, F-44300 Nantes

F. Elefant (corresponding author), A. Babarit and P. Ferrant are with Laboratoire de recherche en Hydrodynamique, Énergétique, et Environnement Atmosphérique, Nantes Université, Ecole Centrale Nantes – C.N.R.S., L.H.E.E.A. F-44300, Nantes, France (e-mails: felix.elefant@ec-nantes.fr, aurelien.babarit@ec-nantes.fr, pierre.ferrant@ec-nantes.fr).

Digital Object Identifier: https://doi.org/10.36688/ewtec-2023-357

the trajectories of these two parts being respectively located above and below the trajectory of eccentric body 2. Distributed in such a way on parallel planes, the eccentric bodies can rotate continuously in opposite directions without colliding with each other, even though their centres of gravity ($G_1$ and $G_2$) move along a same circle.

The angle formed by the half-line $CG_1$ and the longitudinal axis will be denoted $\theta_1$, while the angle formed by the half-line $CG_2$ and the longitudinal axis will be denoted $\theta_2$, as illustrated in Fig. 2.

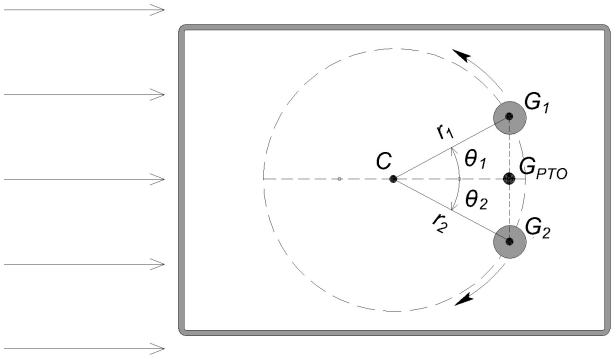


Fig. 2. Trajectory of the gravity centres in horizontal projection.

Throughout the movement, the respective angles of the two bodies are opposite ($\theta_2$=-$\theta_1$), so that the two eccentric bodies rotate symmetrically with respect to the vertical plane containing the longitudinal axis. The total centre of gravity $G_{PTO}$ of both bodies moves back and forth along the longitudinal axis. Furthermore, it can be noted that if the eccentric bodies have a constant rotational speed, the total centre of gravity $G_{PTO}$ exhibits a strictly sinusoidal motion.

When the two half lines $CG_1$ and $CG_2$ are perpendicular with the longitudinal axis ($\theta_1$=-$\theta_2$=±90°), the total centre of gravity $G_{PTO}$ coincides with the centre $C$ of the circle. In this particular situation, which we will call "neutral position", the mass of the PTO is balanced with respect to the centre $C$.

### C. *Main objective of the study*

The purpose of this study is to investigate, through modelling and numerical simulation, the impact of the main parameters, i.e. phase and total mass moment of the PTO, on the performance of a counter-rotating device subjected to regular waves of different heights and wavelengths.

## II. MODELLING OF THE SYSTEM

### D. *Mechanical description of the system*

In the present study, we will consider a terrestrial reference frame $(O, \overrightarrow{x_0}, \overrightarrow{y_0}, \overrightarrow{z_0})$, in which $\overrightarrow{z_0}$ points vertically upwards and $\overrightarrow{x_0}$ gives the direction of wave propagation, and a reference frame $(C, \overrightarrow{x_c}, \overrightarrow{y_c}, \overrightarrow{z_c})$ attached to the floating body, wherein $C, \overrightarrow{x_c}, \overrightarrow{y_c}, \overrightarrow{z_c}$ are defined in such a way that they coincide with $\overrightarrow{x_0}, \overrightarrow{y_0}, \overrightarrow{z_0}$ when the device is at rest in its neutral position.

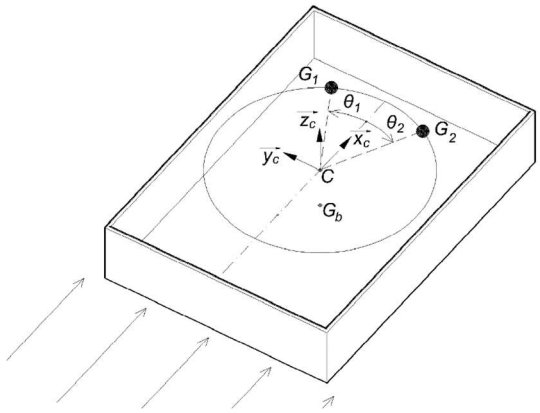


Fig. 3. Coordinate system.

The instantaneous position of the floating body with respect to its neutral position at rest is marked by a generalized coordinate vector $\boldsymbol{X} \overset{\text{def}}{=} [x, y, z, \alpha, \beta, \gamma]^T$, composed of the three translations (surge, sway, heave) and the three Euler angles (roll, pitch, yaw). The angular position of the two rotating bodies is denoted by the angle $\theta_n$, $n \in \{1,2\}$. The total moving mass is denoted $m_{PTO} \overset{\text{def}}{=} m_1 + m_2$.

In the present paper, the oscillating motions of the floating body are linearized. We will therefore only consider the first order terms with respect to the components of the vector $\boldsymbol{X}$ in the Taylor series expansion of the equations of motion. Besides, the rotating masses in the device being capable of performing any number of revolutions around their axis of rotation $(C, \overrightarrow{z_c})$, the angular variables $\theta_1$ and $\theta_2$cannot be described using a finite series expansion.

### E. *Dynamics of the floating body*

After linearization of the floating body motions, the equation of the dynamics of the six-dimensional floating body takes the following form:

$$\boldsymbol{M}_b \ddot{\boldsymbol{X}} = \boldsymbol{F}_{\bar{b}\to b} \tag{1}$$

The matrix $\boldsymbol{M}_b$ represents the generalized mass of the floating body. The vector $\boldsymbol{F}_{\bar{b}\to b}$ denotes the combined external forces acting on the floating body, and results from five contributions:

$$\boldsymbol{F}_{\bar{b}\to b} = \boldsymbol{F}_{res} + \boldsymbol{F}_{moo} + \boldsymbol{F}_{exc} + \boldsymbol{F}_{rad} + \boldsymbol{F}_{pto\to b} \tag{2}$$

1) The term $\boldsymbol{F}_{res}$ is the hydrostatic restoring force. To the first order, it can be written:

$$\boldsymbol{F}_{res} = -\boldsymbol{K}_{res}\boldsymbol{X} \tag{3}$$

with $\boldsymbol{K}_{res}$ the stiffness matrix depending on the geometry of the floating body.

2) In a first approach, we will assume that the mooring force can be approximated locally by a stiffness matrix $\boldsymbol{K}_{moo}$:

$$\boldsymbol{F}_{moo} = -\boldsymbol{K}_{moo}\boldsymbol{X} \tag{4}$$

3) The term $\boldsymbol{F}_{exc}$ represents the excitation force exerted by the incident waves.
4) The motions of the floating body produce radiated waves that disturb the pressure field, resulting in the appearance of a radiative force $\boldsymbol{F}_{rad}$.
5) The term $\boldsymbol{F}_{pto\to b}$ is the force that the PTO exerts on the floating body. It is also the sum of the forces exerted by the two bodies that make up the PTO : $\boldsymbol{F}_{pto\to b} = \sum_{n\in\{1,2\}} \boldsymbol{F}_{n\to b}$

Since the motion of the PTO is nonlinear, it is not possible to solve the system directly in the frequency domain. We have to calculate all the forces, and in particular the hydrodynamic forces $\boldsymbol{F}_{exc}$ and $\boldsymbol{F}_{rad}$, in the time domain.

### *F. Hydrodynamic forces in the time domain*

In a first place, we calculated the hydrodynamic coefficients $\boldsymbol{f}_{exc}(\omega)$ and $\boldsymbol{K}_{rad}(\omega)$ in the frequency domain using the open source code *NEMOH* [7]. This computational code, developed by the *Laboratoire de recherche en Hydrodynamique, Énergétique et Environnement Atmosphérique* (LHEEA) for several years, is based on a Boundary Element Method (BEM) which allows for rapid testing of various configurations.

To determine the time-domain forces from the frequency-domain coefficients, we used the *Marine System Simulator* [8] developed by the Norwegian University of Science and Technology (NTNU), which allows to build a dynamical system (6), whose output $\widehat{\boldsymbol{\mu}}$ provides an approximation of the radiative stress component associated with the fluid memory effect [9]. The remaining radiative stress component comes from $\boldsymbol{M}_{A,\infty}$, i.e. the limit of the added mass matrix when the wave frequency ω tends to infinity:

$$\boldsymbol{F}_{rad} \approx -\boldsymbol{M}_{A,\infty}\ddot{\boldsymbol{X}} - \widehat{\boldsymbol{\mu}} \tag{5}$$

$$\begin{aligned} \dot{\boldsymbol{X}}_{rad} &= \widehat{\boldsymbol{A}}\boldsymbol{X}_{rad} + \widehat{\boldsymbol{B}}\dot{\boldsymbol{X}} \\ \widehat{\boldsymbol{\mu}} &= \widehat{\boldsymbol{C}}\boldsymbol{X}_{rad} + \widehat{\boldsymbol{D}}\dot{\boldsymbol{X}} \end{aligned} \tag{6}$$

In this system, $\boldsymbol{X}_{rad}$ denotes the state vector that reflects the influence of the past on the evolution of the radiative stress. The matrices $\widehat{\boldsymbol{A}},\widehat{\boldsymbol{B}},\widehat{\boldsymbol{C}},\widehat{\boldsymbol{D}}$ are identified by Fossen and Pérez's method [9].

### *G. Dynamics of the rotating masses*

Writing the motion of a rotating mass as the sum of the motion of the floating body and a relative motion, and then linearizing the motions of the floating body, we obtain the following 6-dimensional dynamics equation for each rotating mass:

$$\begin{aligned} \forall n \in \{1,2\},\ \boldsymbol{M}_n\ddot{\boldsymbol{X}} + \ddot{\theta}_n\boldsymbol{J}_n + \dot{\theta}_n^2\boldsymbol{L}_n + 2\dot{\theta}_n\boldsymbol{C}_n\dot{\boldsymbol{X}} \\ = \boldsymbol{F}_{g\to n} + \boldsymbol{F}_{b\to n} \end{aligned} \tag{7}$$

Equation (7) allows us to determine the binding force $\boldsymbol{F}_{b\to n}$ as a function of the system variables, and thus allows us to calculate the force that the PTO exerts on the floating body. In this equation, $\boldsymbol{M}_n$ is the generalized inertia matrix of a body expressed at point $C$, $\ddot{\theta}_n\boldsymbol{J}_n$ is the force induced at point $C$ by the angular acceleration of the body, $\dot{\theta}_n^2\boldsymbol{L}_n$ is the centrifugal force at point $C$ and $\boldsymbol{C}_n$ is the matrix of the Coriolis coefficients of the body. The vectors $\boldsymbol{J}_n$, $\boldsymbol{L}_n$, $\boldsymbol{F}_{g\to n}$ are functions of the angle $\theta_n$ of the body and the rotations of the floating body, while the matrices $\boldsymbol{M}_n$ and $\boldsymbol{C}_n$ depend only on the angle $\theta_n$ of the body.

With respect to the floating body, each rotating mass has one degree of freedom, namely rotation about the axis $(C, \overrightarrow{z_c})$. The equation of motion according to this degree of freedom can be written:

$$\begin{aligned} \mathcal{I}_{Zc,n}\left(\ddot{\gamma} + \ddot{\theta}_n\right) + m_n r_n(\ddot{y}\cos\theta_n - \ddot{x}\sin\theta_n) \\ = c_n - m_n r_n g(\beta\sin\theta_n + \alpha\cos\theta_n) \end{aligned} \tag{8}$$

This equation relates the torque $c_n$ exerted by the electric generator to the motion of an eccentric body through its eccentric moment $m_n r_n$, its moment of inertia $\mathcal{I}_{Zc,n}$ relative to the rotation axis $(C, \overrightarrow{z_c})$, and the acceleration of gravity $g$.

### *H. Canonical equation for the whole device*

In the present study, we wish to observe the response of the system to a given excitation $\boldsymbol{F}_{exc}(t)$ and for a given trajectory $\theta_n(t)$. In other words, $\theta_1$ et $\theta_2$ are input variables along with $\boldsymbol{F}_{exc}$. Combining (1), (2) and (7), we obtain the equation of motion of the floating body $\boldsymbol{X}$:

$$\begin{aligned} \left(\boldsymbol{M}_b + \sum_n \boldsymbol{M}_n\right)\ddot{\boldsymbol{X}} = \boldsymbol{F}_{res} + \boldsymbol{F}_{moo} + \boldsymbol{F}_{exc} + \boldsymbol{F}_{rad} \\ + \sum_n \left(\boldsymbol{F}_{g\to n} - \ddot{\theta}_n\boldsymbol{J}_n - \dot{\theta}_n^2\boldsymbol{L}_n - 2\dot{\theta}_n\boldsymbol{C}_n\dot{\boldsymbol{X}}\right) \end{aligned} \tag{9}$$

In order to solve the dynamics of the device, we need to write the evolution equation of the state vector $\boldsymbol{Y} = [\boldsymbol{X}, \dot{\boldsymbol{X}}, \boldsymbol{X}_{rad}]^t$. By expanding the radiative stress in equation (9) and recombining the terms, we obtain the following canonical equation:

$$\begin{aligned} \dot{\boldsymbol{Y}} \\ = \begin{bmatrix} \boldsymbol{0} & \boldsymbol{I}_6 & \boldsymbol{0} \\ -\boldsymbol{M}^{-1}\boldsymbol{K} & -\boldsymbol{M}^{-1}\widehat{\boldsymbol{D}} & -\boldsymbol{M}^{-1}\widehat{\boldsymbol{C}} \\ \boldsymbol{0} & \widehat{\boldsymbol{B}} & \widehat{\boldsymbol{A}} \end{bmatrix}\boldsymbol{Y} \\ + \begin{bmatrix} \boldsymbol{0} \\ \boldsymbol{M}^{-1}\left(\boldsymbol{F}_{exc} + \sum_n \left(\boldsymbol{F}_{g\to n} - \ddot{\theta}_n\boldsymbol{J}_n - \dot{\theta}_n^2\boldsymbol{L}_n - 2\dot{\theta}_n\boldsymbol{C}_n\dot{\boldsymbol{X}}\right)\right) \\ \boldsymbol{0} \end{bmatrix} \end{aligned} \tag{10}$$

where $\boldsymbol{I}_6$ denotes the identity matrix of dimension 6x6.

$$\boldsymbol{M} = \boldsymbol{M}_b + \sum_n \boldsymbol{M}_n + \boldsymbol{M}_{A,\infty}\ ;\ \boldsymbol{K} = \boldsymbol{K}_{res} + \boldsymbol{K}_{moo} \tag{11}$$

## III. NUMERICAL MODEL AND SIMULATIONS

### I. *Study protocol*

The aim of our simulation work is to study the influence of different parameters through the example of a floating body of elementary geometry. To do so, we solved (10) in the time domain with Matlab. Then, we compared the results obtained for different values of the PTO phase and for different body masses, while the device is subjected to different regular waves.

### J. *Numerical model of the device*

#### 1) *Characteristics of the floating body*

The floating body of the device under consideration is a box having the following dimensions: length $l_b$ = 45 m, width $w_b$ = 20 m, draught $h_b$ = 6.67 m. The dimensions of the hull are such that the pitching excitation force reaches its maximum for a wave period of 9 s, which typically corresponds to the centre of the useful period range for a wave energy converter. Since the floating body is symmetrical with respect to the plane $(O, \overrightarrow{x_0}, \overrightarrow{z_0})$, the description of one half of its geometry is sufficient to calculate the hydrodynamic coefficients. A half floating body is modelled by a mesh consisting of 278 quadrangular panels, as shown in Fig. 4.

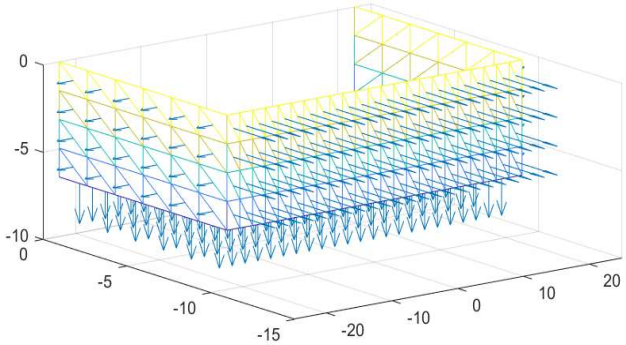


Fig. 4. Mesh of a half floating body.

#### 2) *Characteristics of the ballast*

We assume that the hull of the floating body is made of steel and has a constant thickness of 20 mm over its entire wetted surface. We take as reference 8000 kg/m³ for the density of the steel, which allows us to determine the generalized hull mass matrix $\boldsymbol{M}_h$. The sum of the PTO mass $m_{PTO}$ and the hull mass $m_h$ is less than the desired displacement $\rho_0 \mathcal{V}_0$. A ballast of mass $m_l$ is required to achieve the desired draft:

$$m_l = \rho_0 \mathcal{V}_0 - m_h - m_{PTO} \tag{12}$$

In order to obtain a pitch resonance frequency $\omega_{r5}$ as low as possible, the ballast is composed of two cast iron blocks of density 5500 kg/m³ which are spaced apart so as to maximize the moment of inertia of the floating body with respect to the pitch axis $(C, \overrightarrow{y_c})$.

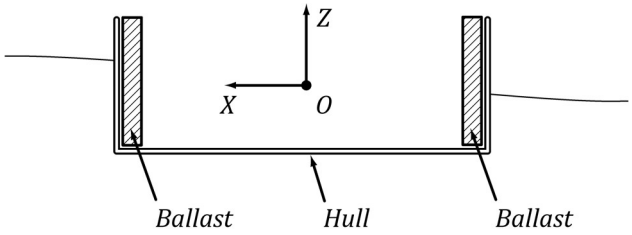


Fig. 5. Mesh of a half floating body.

#### 3) *Characteristics of the PTO*

The centre $C$ of the PTO is located in the centre of the water plane area. The rotating masses are steel blocks of density 8000 kg.m$^{-3}$. The outer surface of the volume swept by the rotating masses passes as close as possible to the inner wall of the hull. The eccentric radius $r_n$, i.e. the distance between the centre of gravity of a body and the centre of the PTO, is fixed at 6.67 m.

In a first place, we have explored the performance of a PTO consisting of two 139-ton rotating masses.

### K. *Simulated time response*

First, we simulate the response to regular waves of period $T$ = 10 s, height $H$ = 2 m, and propagating along the direction $(0, \overrightarrow{x_0})$.

In this simulation (Fig. 6), the two bodies of the device are animated by rigorously symmetrical movements and performed at constant speed to produce a sinusoidal displacement of the centre of gravity $G_{PTO}$ along the longitudinal axis:

$$\begin{cases} \theta_1(t) = +\omega t + \varphi_{PTO} \\ \theta_2(t) = -\omega t - \varphi_{PTO} \end{cases} ; \quad \varphi_{PTO} = \varphi_{exc} + \Delta\varphi \tag{13}$$

The phase of the excitation force is denoted $\varphi_{exc}$, while the motion of the PTO has a phase offset $\Delta\varphi$ with respect to the excitation force. At the initial instant, the floating body is at rest $\dot{\boldsymbol{X}} = [0,0,0,0,0,0]^t$ in its neutral equilibrium position $\boldsymbol{X} = [0,0,0,0,0,0]^t$.

In Fig. 6, we can see that heave and pitch tend to oscillate with the same frequency as the waves, but that surge also exhibits a low frequency oscillation. A plausible cause for the appearance of this oscillation is that the mooring is excited during the transient regime following the initial state: the frequency of the observed oscillation coincides with the surge resonance frequency of the mooring system. Such a low frequency is only weakly damped, so that the amplitude of the low-frequency motion of the surge does not decrease perceptibly over the duration of the simulation. The steady state is therefore not fully reached at the end of the simulation.

However, in order to keep the calculation time reasonable, we considered that the operating regime of the device was sufficiently established from 500 s onwards for us to observe the performance of the device.

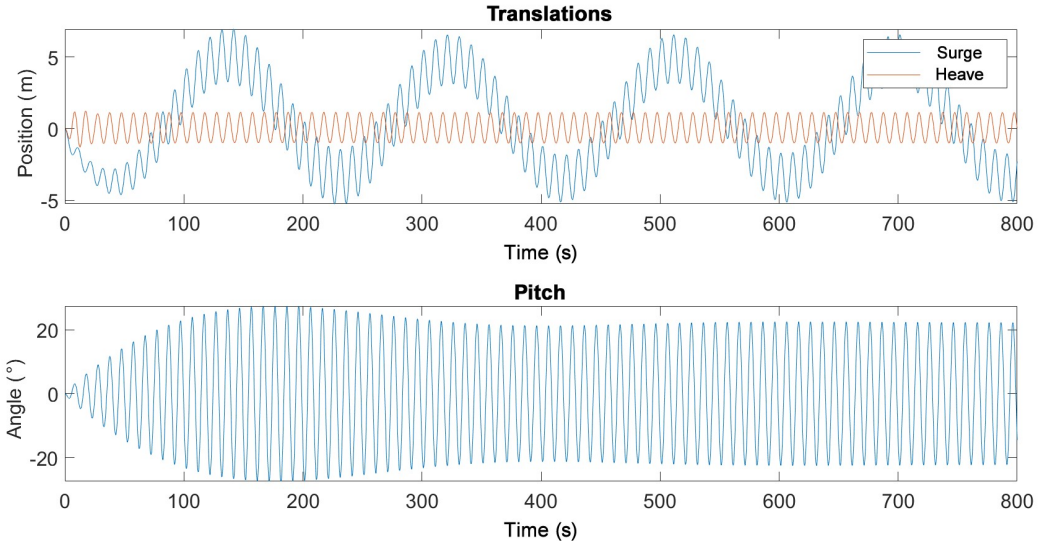


Fig. 6. Oscillations of the float.

### L. *Influence of the PTO phase*

The PTO phase $\varphi_{PTO}$ is of crucial importance for the power capture. To highlight this point, we plot the power produced by the device under the same conditions as before ($T$ = 10 s, $H$ = 2 m, $m_{PTO}$ = 278 t), but for different values of the phase offset $\Delta\varphi$ with respect to the excitation force (see Fig. 7). The simulation covers the time interval $[0, t_f]$. To limit the influence of the transient regime, we calculate the captured power by dividing the energy produced over an interval of the form $[t_f - \Delta t, t_f]$ by the time span $\Delta t$. This time span $\Delta t$ is chosen to correspond to a multiple of the excitation period $T_{exc}$, this multiple being as close as possible to $2/3t_f$.

The power output has a single maximum and a single minimum over [-180°,+180°]. When the power output is negative, the device loses more energy by radiation than it extracts from the incident waves. Furthermore, we note that the minimum is more negative than the maximum is positive (see Fig. 7).

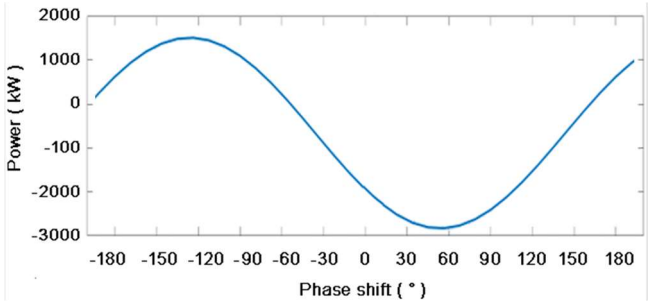


Fig. 7. Power output as a function of the PTO phase offset.

We will note $\Delta\varphi_{opt}$ the optimal value of the phase offset $\Delta\varphi$ for a given set of parameters ($T$,$H$,$m_{PTO}$). Let us specify that the time response illustrated in Fig. 6 corresponds to the optimal phase offset for the considered parameter set.

Fig. 8 presents the evolution of the optimal phase offset $\Delta\varphi_{opt}$ as a function of the period and height of the incident wave.

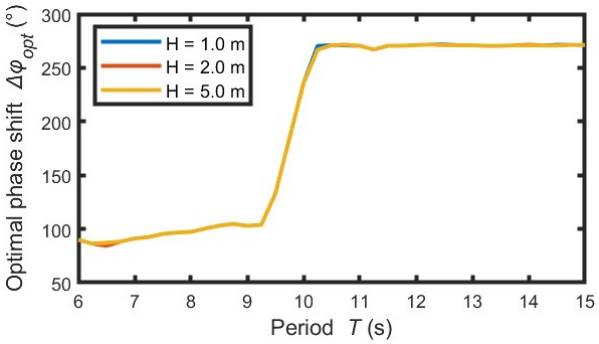


Fig. 8. Optimal phase offset as a function of the wave period.

In Fig. 8, the curves of the optimal phase offset for the different wave heights merge. The wave height has therefore no influence on $\Delta\varphi_{opt}$. The same is true for the mass of the PTO, which we found during the simulations to have no influence on $\Delta\varphi_{opt}$ (this point will be explained analytically in subsection *N*).

We conclude that the optimal phase offset $\Delta\varphi_{opt}$ depends only on the incoming wave period $T$.

Fig. 8 shows that the optimal phase offset $\varphi_{opt}$ passes through 180° with a steep slope near the pitch resonance period $T_{r5}$:

$$T_{r5} = 2\pi\sqrt{\frac{M_{c,55} + M_{A,55} + 2m_l r_l^2 + \sum_n M_{n,55,nt}}{K_{res,55} + K_{moo,55}}} \quad (14)$$

In the preceding expression, $M_{n,55,nt}$ denotes the inertia of the PTO with respect to the pitch axis $(C, \overrightarrow{y_c})$, when the device is in the neutral position. For the considered device, the pitch resonance period $T_{r5}$ is 9.56 s.

The 180° value of the optimal phase offset at resonance is explained by the fact that the floating body oscillates in phase with the pitch excitation force [10], as the inertial forces and the restoring forces acting on the floating body neutralize each other. Thus, the inclination of the floating body has a phase delay of 90° with respect to the inclination of the water surface.

Under these conditions, the optimal phase offset $\Delta\varphi_{opt}$ for the PTO is 180°, as illustrated in Figure 9.

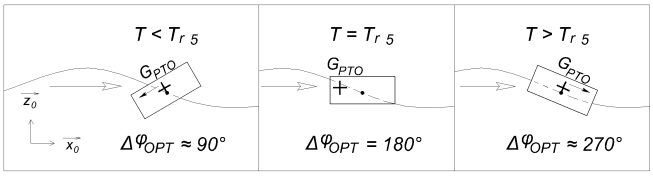


Fig. 9. Schematic view of the device pitching sequence as a function of the wave period.

For excitation periods greater than $T_{r5}$, the restoring forces is much greater than the inertial forces, so that the pitch of the floating body tends to be in phase with the local inclination of the water surface. In this case, the optimal phase offset $\Delta\varphi_{opt}$ tends towards 270°, which corresponds to the location on the circle of axis $(C, \vec{z_c})$ where the downward slope is the strongest.

Conversely, when the excitation period is less than $T_{r5}$, the inertial forces are dominant, and the pitch of the floating body lags behind the local tilt of the water. In this context, the position that maximises the slope in which the PTO mass is located corresponds to a phase offset between +90° and 180°.

In order to make the best use of the available power, the PTO has to be driven such as to verify $\Delta\varphi = \Delta\varphi_{opt}(T)$. In all the following simulations, we will therefore set $\Delta\varphi_{opt}(T)$ as the value for the phase offset $\Delta\varphi$, and observe the influence of parameters other than the phase on the performance of the device.

### *M. Analysis of operation at optimal phase offset*

The behaviour of the device operating at optimal phase offset has been simulated for different wave frequencies and different wave heights. In each simulation performed, the fast Fourier transform of the floating body motions exhibits a distinctive peak at the frequency of the incident waves. The surge presents a secondary peak at mooring resonance frequency.

#### *4) Response amplitude operators*

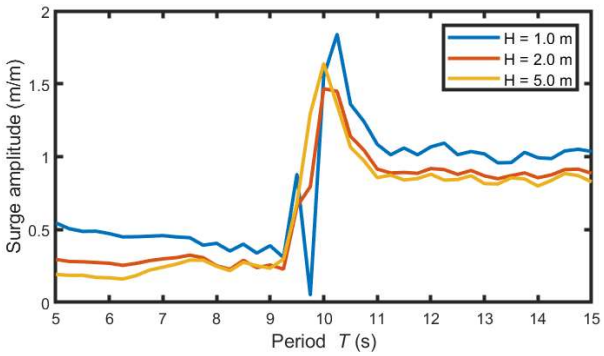


Fig. 10. Surge response amplitude operator.

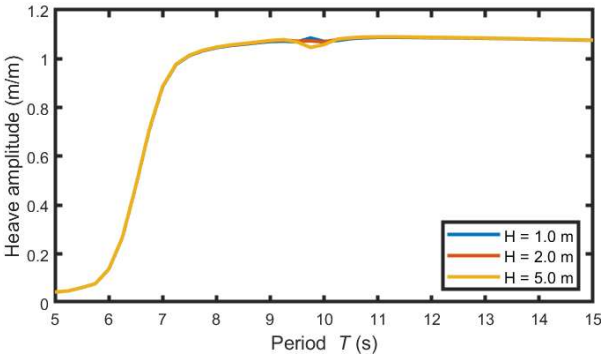


Fig. 11. Heave response amplitude operator.

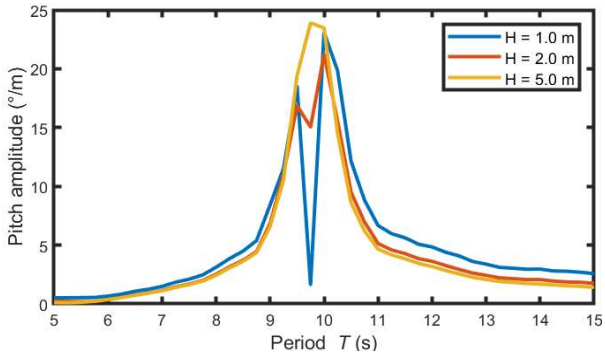


Fig. 12. Pitch response amplitude operator.

In the pitch RAO (Fig. 12), it can be seen that the yellow curve, which corresponds to a wave height of 5.0 meters, reaches its maximum at the resonance period $T_{r5}$, which is consistent with the expected result. However, the red curve and even more so the blue curve exhibits two peaks on either side of the resonance and a trough centred at resonance.

#### *5) Absorbed power*

The behaviour we have just observed in the pitch curves (Fig. 12) is also clearly apparent on the power curves shown in Fig. 13.

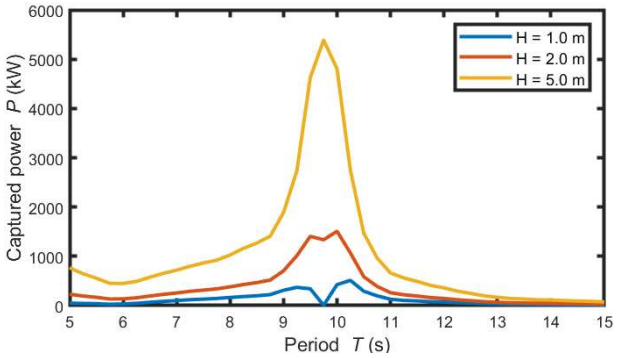


Fig. 13. Power absorbed by the device.

As in subsection *L*, the absorbed power is the mean of the power converted by the PTO over an integral number of cycles, once the oscillation regime is fully established.

Fig. 13 suggests that, at the pitch resonance frequency, the studied device is best suited for certain wave heights. To compare the device performance for different wave heights, a normalization is required.

To this purpose, we divide the captured power by the theoretical maximum power for a symmetrical floating body oscillating in pitch:

$$P_{the} = \frac{\lambda}{\pi} J_i \tag{15}$$

where $\lambda/\pi$ is the maximum capture width for a pitching body and $J_i$ is the incident power per unit front width [10], given by:

$$J_i = \frac{\rho g^2}{32\pi} T H^2 \tag{16}$$

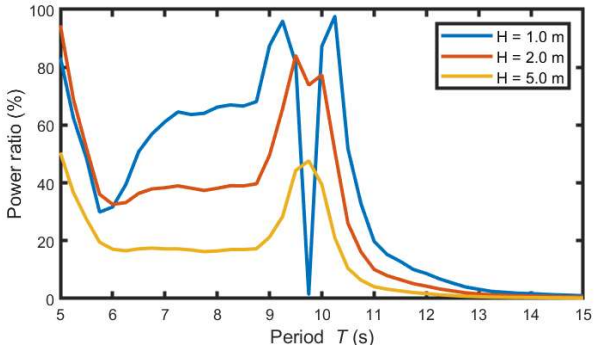


Fig. 14. Ratio of the absorbed power to the theoretical maximum.

## N. *Analytical explanations*

### 6) *Simplified pitching model*

The behavior of the device near the resonance frequency, which may seem surprising in a first place, becomes clearer if we look at the analytical structure of the pitching dynamics. To this end, we temporarily adopt two simplifying hypotheses. Firstly, we assume that the coupling with the other oscillation modes has a negligible effect on the dynamics of the pitch near $T_{r5}$. Secondly, we assume that the nonlinear inertial forces introduced by the PTO are negligible compared with the inertial forces involved in the pitch near $T_{r5}$. In the time domain, the pitch equation is therefore written:

$$M_{55}\ddot{\beta} = -K_{55}\beta - K_{rad,55} * \dot{\beta} + \frac{H}{2} f_{exc,5} + U \tag{17}$$

where $U$ denotes the weight moment of the PTO about the pitch axis:

$$U = \sum_n m_n r_n g \cos\theta_n \tag{18}$$

The two bodies of the PTO move symmetrically, so that $U$ can be expressed as a function of $\theta_1$ only:

$$U = 2 m_1 r_1 g \cos\theta_1 \tag{19}$$

Equation (17) is linear with respect to both input variables, $U$ and $\beta$. It is therefore possible to study the system in the frequency domain.

We introduce the notation $F_{e,5}(\omega)$ for the Fourier transform of the excitation force, the notation $U(\omega)$ for the transform of the PTO's weight, the notation $M'_{55}(\omega)$ for the total inertia with respect to the pitch axis, added mass included, and the notation $R_{55}(\omega)$ for the radiative damping diagonal coefficient for the pitch axis:

$$\beta(\omega) = \frac{F_{e,5}(\omega) + U(\omega)}{K_{55} - \omega^2 M'_{55}(\omega) + j\omega R_{55}(\omega)} \tag{20}$$

where $F_{e,5}(\omega)$ is defined as follows:

$$F_{e,5}(\omega) = \frac{H}{2} f_{exc,5}(\omega) \tag{21}$$

In (20), the pitch dynamics takes the form of a damped oscillator subjected to external disturbances.

### 7) *Analytical power capture formula*

A method for calculating the power captured by an oscillating system is given by Falnes in [10]. We will only recall the main steps of this method.

The power conceded to the device by the wave excitation force is:

$$P_e(\omega) = {}^1\!/_2\, \Re\left( j\omega\, \beta(\omega)\, F^*_{e,5}(\omega) \right) \tag{22}$$

where $\Re$ denotes the real part operator.

The power radiated by the device due to its pitch motion is determined from the radiation damping coefficient:

$$P_r(\omega) = {}^1\!/_2\, \omega^2 R_{55}(\omega) |\beta(\omega)|^2 \tag{23}$$

The power captured by the pitch is the difference between the power extracted from the incident wave and the power lost by radiation:

$$P(\omega) = P_e(\omega) - P_r(\omega) \tag{24}$$

The power can be written in the following form, in which, for readability reasons, the "$(\omega)$" are implied:

$$P = \omega \frac{Q_{55}\Im\left(UF^*_{e,5}\right) - \omega R_{55}\left(|U|^2 + \Re\left(UF^*_{e,5}\right)\right)}{2|Q_{55} - j\omega R_{55}|^2} \tag{25}$$

where $\Im$ denotes the imaginary part operator and $Q_{55}$ is:

$$Q_{55} = \omega^2 M'_{55} - K_{55} \tag{26}$$

### 8) *Relationship to the phase and the amplitude of the rotary motion*

To study the performance of our device, it is convenient to express the captured power as a function of the PTO phase offset $\Delta\varphi$ and the PTO weighing moment.

To this end, we introduce the amplitude parameter $\sigma$:

$$\sigma = \frac{|U|}{|F_{e,5}|} \tag{27}$$

After a few lines of calculation, (25) simplifies to:

$$P = \omega|F_{e,5}|^2 \frac{Q_{55}\sigma \sin(\Delta\varphi) + \omega R_{55}\left(\frac{1}{4} - \left|\frac{1}{2} + \sigma e^{j\Delta\varphi}\right|^2\right)}{2|Q_{55} - j\omega R_{55}|^2} \tag{28}$$

From (28), it is possible to determine a theoretical value for the phase and amplitude optimum of the motion of the eccentric bodies.

*9) Theoretical optimal phase offset*

Based on the present model, we search for the optimal theoretical phase offset, denoted as $\Delta\varphi_{the}$.

First, we look for local extrema of the captured power by taking the partial derivate of (28) with respect to the phase offset $\Delta\varphi$. Cancellation of the power partial derivate leads to the following relationship:

$$sin(\Delta\varphi_{the}) = -\frac{\omega^2 M'_{55} - K_{55}}{\omega R_{55}} cos(\Delta\varphi_{the}) \tag{29}$$

To proceed with the resolution, we will show that $cos(\Delta\varphi_{the})$ is non-zero. To this end, we take the square of (29) and add $cos^2(\Delta\varphi_{the})$ to both members of the equation:

$$1 = \left[1 + \left(\frac{\omega^2 M'_{55} - K_{55}}{\omega R_{55}}\right)^2\right] cos^2(\Delta\varphi_{the}) \tag{30}$$

From (30), it is obvious that $cos(\Delta\varphi_{the})$ is not zero. Therefore, we can divide both members of (29) by $cos(\Delta\varphi_{the})$, to express the tangent:

$$tan(\Delta\varphi_{the}) = -\frac{\omega^2 M'_{55} - K_{55}}{\omega R_{55}} \tag{31}$$

Equation (31) defines the theoretical optimum $\Delta\varphi_{the}$:

$$\exists k \in \mathbb{Z}, \Delta\varphi_{the} = k\pi - arctan\left(\frac{\omega^2 M'_{55} - K_{55}}{\omega R_{55}}\right) \tag{32}$$

Without loss of generality, we can restrict our study to phase angles within $]-90°, +270°]$. We will denote $\Delta\varphi_a$ and $\Delta\varphi_b$ the two extrema within this range.

$$\Delta\varphi_a = -arctan\left(\frac{\omega^2 M'_{55} - K_{55}}{\omega R_{55}}\right) \quad ; \quad \Delta\varphi_b = \Delta\varphi_a + \pi \tag{33}$$

To determine which phase offset is optimal, we compare the captured power for $\Delta\varphi_a$ and $\Delta\varphi_b$:

$$\Delta P = P(\Delta\varphi_a) - P(\Delta\varphi_b) \tag{34}$$

We use (28), (29) and (33) to develop (34) and express the power difference $\Delta P$ as a function of $\cos(\Delta\varphi_a)$:

$$\Delta P = -\omega|F_{e,5}|^2 \sigma \frac{\frac{Q_{55}^2}{\omega R_{55}} + \omega R_{55}}{|Q_{55} - j\omega R_{55}|^2} \cos(\Delta\varphi_a) \tag{35}$$

Equation (35) shows that the sign of the power difference $\Delta P$ is the opposite of the sign of $\cos(\Delta\varphi_a)$. According to its definition, $\Delta\varphi_a$ is within $]-90°, +90°[$, which means that $\cos(\Delta\varphi_a)$ is positive.

We conclude that $\Delta P$ is negative. Therefore $\Delta\varphi_b$ is the theoretical optimal phase offset $\Delta\varphi_{the}$:

$$\Delta\varphi_{the} = \pi - arctan\left(\frac{\omega^2 M'_{55} - K_{55}}{\omega R_{55}}\right) \tag{36}$$

We note that the theoretical optimal phase offset is independent from the wave height $H$, and depends only on the circular frequency $\omega$, which is consistent with our previous observations (see subsection *L*).

In Fig. 15, we superimposed the optimal phase offsets obtained respectively by simulation (Fig. 8) and analytically (see 36) from our simplified model.

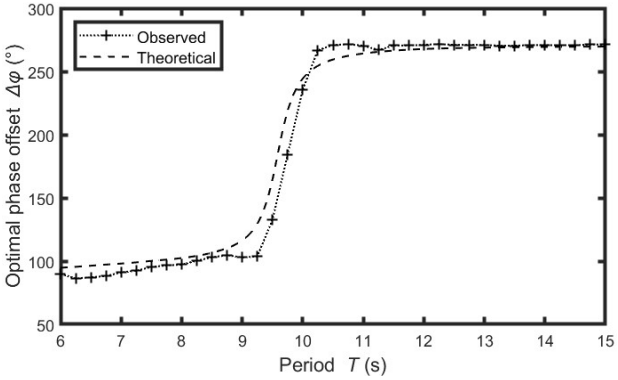


Fig. 15. Comparison between simulated and analytical phase offset optima over the period range.

Fig. 15 shows a reasonable agreement between the two curves.

*10) Theoretical optimal amplitude ratio*

A theoretical optimum for the amplitude ratio is denoted $\sigma_{the}$. Using (28), we look for the points where the partial derivative of the power with respect to the amplitude ratio $\sigma$ is zero. After a few lines of calculations, we obtain the following relationship:

$$\sigma_{the} = \frac{\omega^2 M'_{55} - K_{55}}{2\omega R_{55}} sin(\Delta\varphi) - \frac{1}{2} cos(\Delta\varphi) \tag{37}$$

We can see that $\sigma_{the}$ is a function of the phase offset $\Delta\varphi$. To investigate further, we focus on $\sigma_{the}$ when $\Delta\varphi$ is optimal.

Using (30) and the negativity of $\cos(\Delta\varphi_{the})$, due to (36), we have:

$$\cos(\Delta\varphi_{the}) = -\frac{1}{\sqrt{1+\left(\frac{\omega^2 M'_{55}-K_{55}}{\omega R_{55}}\right)^2}} \tag{38}$$

We now use (29) and (38) to express $\sin(\Delta\varphi_{the})$:

$$\sin(\Delta\varphi_{the}) = \frac{\frac{\omega^2 M'_{55}-K_{55}}{\omega R_{55}}}{\sqrt{1+\left(\frac{\omega^2 M'_{55}-K_{55}}{\omega R_{55}}\right)^2}} \tag{39}$$

Using (38) and (39) in (37) leads to:

$$\sigma_{the} = \frac{1}{2}\sqrt{1+\left(\frac{\omega^2 M'_{55}-K_{55}}{\omega R_{55}}\right)^2} \tag{40}$$

### O. *Special case study*

*Case 1:* $\omega \ll \omega_{r5}$

We observe that if the circular frequency $\omega$ is small with respect to the resonance frequency $\omega_{r5}$, the dynamics is dominated by the stiffness $K_{55}$:

$$P \sim \frac{\omega|F_{e,5}|^2}{2K_{55}}\sigma\sin(-\Delta\varphi) \tag{41}$$

In this case, the optimal phase offset $\Delta\varphi_{the}$ tends towards 270°, which is consistent with Fig. 8. When $\omega$ is small enough, the amplitude ratio $\sigma$ gains to be as large as possible in order to maximize power extraction $P$. To operate efficiently on long waves, the device therefore gains from having as large an eccentric moment as possible.

*Case 2:* $\omega \approx \omega_{r5}$

When the circular frequency is close to the resonance frequency $\omega_{r5}$, the radiation coefficient $R_{55}$ dominates the pitch dynamics:

$$P \sim \frac{|F_{e,5}|^2}{2R_{55}}\left(\frac{1}{4}-\left|\frac{1}{2}+\sigma e^{j\Delta\varphi}\right|^2\right) \tag{42}$$

In this case, the optimal phase offset is 180°. Rewriting equation (42) for the optimal phase offset $\Delta\varphi = \Delta\varphi_{the} =$ 180°, we obtain:

$$P \sim \frac{|F_{e,5}|^2}{2R_{55}}\sigma(1-\sigma) \tag{43}$$

Our simplified analytical model thus predicts that the optimal amplitude ratio at resonance is:

$$\sigma_{the}(\omega_{r5}) = ½ \tag{44}$$

At resonance, there is a relationship between the optimum mass of the PTO and the height $H$ of the wave :

$$m_{PTO,the} = 2m_{1,opt} = \frac{Hf_{exc,5}(\omega_{r5})}{4r_1 g} \tag{45}$$

We observe that the power produced near the resonance frequency is very sensitive to the amplitude parameter $\sigma$, especially when the mass of the PTO exceeds the optimum mass. According to (43), our simplified analytical model predicts that a mass twice as large as the optimal mass is enough to cancel out the power capture of the device at resonance.

As an illustration, (43) predicts that, for a wave height $H$ = 1 m, the mass $m_{PTO}$ = 278 t is too high to produce power. This prediction is in agreement with the simulation results: one can refer to the blue curve of Fig. 13 for confirmation.

*Case 3:* $\omega > \omega_{r5}$

In this case, the pitch inertia $M'_{55}$ is dominant. The optimal phase is between +90° and +180°, and the optimal value for the PTO mass is larger than at resonance.

#### 11) *Summary of the lessons learned from the simple model*

In the power formula given by equation (28), the denominator evolves favourably as the resonance is approached, which is illustrated by the yellow curve in Fig. 13 and Fig. 14. In the immediate vicinity of resonance, the numerator is dominated by the damping term. This term evolves unfavourably if the magnitude of the mass moment is not adapted to the excitation force. This situation is illustrated by the blue curve, which shows power drop centred at resonance. The ability to adapt the mass moment of the PTO would therefore be useful.

### P. *Influence of the PTO mass at resonance frequency*

To complete our study, we simulated the effect of the PTO mass on the performance of the device at resonance as a function of incident wave height, as shown in Fig. 16.

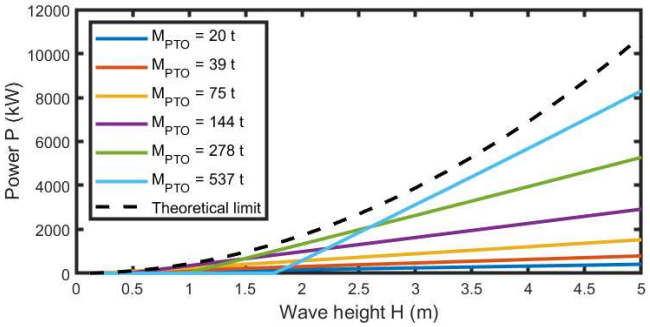


Fig. 16. Power output for different masses at resonance.

We then compared the observed optimal mass for each height with the theoretical mass from equation (45), as shown in Fig. 17.

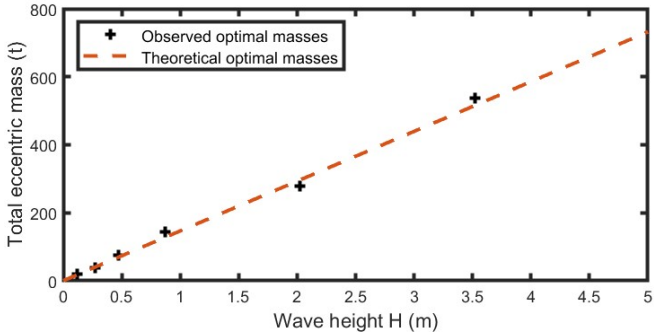


Fig. 17. Optimal mass as a function of the incident wave height.

Fig. 17 confirms the good agreement between the simulation results of the nonlinear model (10) and the predictions of the simplified model for pitching (17).

## IV. CONCLUSION AND PROSPECTS

### Q. *Summary of the study*

In the present study, the performance of a wave energy conversion device with counter-rotating masses has been explored. In a first step, a dynamic model that is linear with respect to the motion of the floating body and nonlinear with respect to the PTO motion was developed. In the time domain, this model translates into a system of nonlinear differential equations that was solved numerically. In a second step, the time response of the device was simulated for different monochromatic waves. In a third step, it was shown that there is an optimal phase and amplitude for the mass moment of the PTO.

At frequencies far from resonance, the mass moment is best kept as large as possible. However, close to resonance, a mass moment that is too large is unfavourable for power collection. A simple analytical model limited to the pitch dynamics validated these results.

### R. *Research perspectives*

In addition to the work presented above, it would be useful to estimate the average power produced over one year of operation for one or more reference sites. To this end, the present study could be extended by exploring the performance of the device in response to different irregular waves.

Given the magnitude of the motions of the floating body, it would be interesting to study the effect of terms of order higher than one on the performance of the device. It could also be interesting to couple the non-linear PTO with a fully non-linear hydrodynamic model in time-domain.

## REFERENCES

[1] A. F. d. O. Falcao, «Wave energy utilization : a review of technologies,» *Renewable and sustainable Energy Reviews,* vol. 14, n° %13, pp. 889-918, 2010.

[2] M. H. Chen, D. R. Delbalzo, «Dynamic buoy effects on a sliding wave energy converter with eSpring control», *OCEANS 2016 - Shanghai*, Shanghai, 2016.

[3] P. Sincock, A. C. Eassom, S. J. Wales, H. Marcollo, «Wave energy converter». Patent WO/2018/053602, 2018.

[4] A. Clement, A. Babarit, G. Duclos, « Apparatus for converting wave energy into electric power ». Patent WO/2006/040341, 2007.

[5] V. Vamvas, «Eccentrically Rotating Mass Turbine». Patent US20210285415, 2021.

[6] F. Elefant, A. Elefant, «Wave energy converter exploiting the orbital movement of a heavy carriage». Patent WO/2015/121551 A2, 2015.

[7] A. Babarit, G. Delhommeau, «Theoretical and numerical aspects of the open source BEM solver NEMOH,» *11th European Wave and Tidal Energy Conference (EWTEC 2015)*, Nantes, France, 2015.

[8] T. Perez, O. Smogelli, T. Fossen, A. Sorensen, «An Overview of the Marine Systems Simulator (MSS): A Simulink Toolbox for Marine Control Systems,» *Modeling, Identification and Control,* vol. 27, n° %14, pp. 259-275, 2006.

[9] T. Perez, T. Fossen, «Time-vs. frequency-domain identification of parametric radiation force models for marine structures at zero speed,» *Modeling, Identification and Control,* vol. 29, n° %11, pp. 1-19, 2008.

[10] J. Falnes, Ocean Waves and Oscillating Systems, Cambridge: Cambridge University Press, 2002.